

UNCLASSIFIED

*Insights on Compressive Damage
Development in Glass*

Kathryn A. Dannemann

Sidney Chocron

Charles E. Anderson, Jr.

James F. Spencer

Contract: W56HZV-06-C-0194

SwRI[®] Report 18.12544/028

Prepared for:

US Army RDECOM-TARDEC

RDTA-RS

Warren, MI 43897-5000

March 2011

UNCLASSIFIED

UNCLASSIFIED

UNCLASSIFIED



REPORT DOCUMENTATION PAGE			<i>Form Approved</i> OMB No. 0704-0188		
Public reporting burden for this collection of information is estimated to average 1 hour per response, including the time for reviewing instructions, searching data sources, gathering and maintaining the data needed, and completing and reviewing the collection of information. Send comments regarding this burden estimate or any other aspect of this collection of information, including suggestions for reducing this burden to Washington Headquarters Service, Directorate for Information Operations and Reports, 1215 Jefferson Davis Highway, Suite 1204, Arlington, VA 22202-4302, and to the Office of Management and Budget, Paperwork Reduction Project (0704-0188) Washington, DC 20503. PLEASE DO NOT RETURN YOUR FORM TO THE ABOVE ADDRESS.					
1. REPORT DATE (DD-MM-YYYY) 31-03-2011		2. REPORT TYPE Technical		3. DATES COVERED (From - To) July 2009 – March 2011	
4. TITLE AND SUBTITLE Insights on Compressive Damage Development in Glass			5a. CONTRACT NUMBER W56HZV-06-C-0194		
			5b. GRANT NUMBER		
			5c. PROGRAM ELEMENT NUMBER		
6. AUTHOR(S) Kathryn A. Dannemann, Sidney Chocron, Charles E. Anderson, Jr., James F. Spencer			5d. PROJECT NUMBER 18.12544		
			5e. TASK NUMBER		
			5f. WORK UNIT NUMBER		
7. PERFORMING ORGANIZATION NAME(S) AND ADDRESS(ES) Southwest Research Institute P. O. Drawer 28510 San Antonio, TX 78228-0510;			8. PERFORMING ORGANIZATION REPORT NUMBER 18.12544/028		
9. SPONSORING/MONITORING AGENCY NAME(S) AND ADDRESS(ES) US Army Tank-Automotive Research, Development, and Engineering Center, Warren, MI 48397-5000			10. SPONSOR/MONITOR'S ACRONYM(S) RDECOM-TARDEC/RDTA-RS		
			11. SPONSORING/MONITORING AGENCY REPORT NUMBER		
12. DISTRIBUTION AVAILABILITY STATEMENT Approved for Public Release; Unlimited Distribution					
13. SUPPLEMENTARY NOTES The views, opinion, and/or findings contained in this report are those of the authors and should not be construed as an official Department of the Army position, policy, or decision, unless so designated by other documents.					
14. ABSTRACT Post-test microscopy evaluations were performed on borosilicate (Borofloat® 33) and soda-lime (Starphire®) glass specimens following confined compression tests. These included optical and electron microscopy investigations of select specimens tested at low strain rates with confinement pressures up to 1 GPa. Specimens were evaluated following removal of the confinement sleeve or holder. The objective of this work was to investigate the flow and failure behavior of both glasses due to compressive loading with confinement. The observations provide insight into the damage process that occurs during projectile impact/penetration into transparent armor. Highlights of the microscopy evaluations are compared and contrasted for the two glasses of interest.					
15. SUBJECT TERMS borosilicate glass, Starphire glass, compression, damage, microscopy, confinement, comminution					
16. SECURITY CLASSIFICATION OF:			17. LIMITATION OF ABSTRACT None	18. NUMBER OF PAGES 36	19a. NAME OF RESPONSIBLE PERSON Frederick C. Rickert
a. REPORT Unlimited	b. ABSTRACT Unlimited	c. THIS PAGE Unlimited			19b. TELEPHONE NUMBER (Include area code) 586-282-3914

UNCLASSIFIED



Table of Contents

	Page
1.0 Introduction.....	1
2.0 Materials	3
3.0 Experimental Procedure.....	5
3.1 Specimen Preparation.....	5
3.2 Confined Compression Tests	6
3.3 Post-Test Specimen Evaluation.....	6
4.0 Results.....	9
5.0 Discussion.....	13
6.0 Summary.....	21
7.0 Acknowledgements.....	23
8.0 References.....	25

UNCLASSIFIED



UNCLASSIFIED

List of Figures

	Page
Figure 1. Pre-damaged Borofloat specimen (BF-45 end and side view) following a thermal shock treatment. The crack pattern is representative of the pre-damaged BF specimens.....	5
Figure 2. Pre-damaged Starphire specimen (SP-6) showing representative damage pattern for the Starphire glass specimens following the thermal shock procedure.	5
Figure 3. Removal of the confining sleeve/holder was necessary to view in-situ damage following compression testing of. (a) Confined sleeve specimen – end view (b) Triaxial compression specimens (B52_3) – lengthwise view.....	7
Figure 4. Axial stress-strain response of intact and pre-damaged Borofloat (blue curves) and Starphire (red curves) specimens tested in triaxial compression.....	9
Figure 5. Equivalent stress vs. hydrostatic pressure comparison plot for <i>intact</i> Borofloat and Starphire glass specimens for data obtained from confined (bomb intact) and unconfined tests [32].....	11
Figure 6. Equivalent stress vs. hydrostatic pressure comparison plot obtained from confined compression test data on <i>pre-damaged</i> Borofloat and Starphire glass specimens [32].....	11
Figure 7. Pre-damaged Borofloat and Starphire specimens following monotonic loading with hydraulic confining pressures of (a) 25 MPa, (b) 100 MPa, (c) 250 MPa, (d) 400 MPa. The dominant shear plane is marked in each photograph. Orientation of the shear plane is 55-70° from the loading axis for Borofloat, and 50-60° for Starphire. The equivalent stress and hydrostatic pressure (in red box) correspond to the data plotted in Figure 6.....	14
Figure 8. Dominant shear plane (red arrow) and secondary damage regions (black arrow) formed during confined sleeve testing of: a) Borofloat (BF-37): Max σ_{eq} = 2210 MPa, Max $\bar{\sigma}_r$ = 870 MPa; Max P = 1580 MPa	15
Figure 9. Starphire specimen (SP-8, $\bar{\sigma}_r$ = 100 MPa) following compression testing with hydraulic confinement. (a) As tested. (b) Identical specimen following gold coating.....	15
Figure 10. Rounded particles in the vicinity of the shear plane for Borofloat specimens tested with hydraulic confinement. (a) Specimen BF-88: $\bar{\sigma}_r$ = 250 MPa, max P = 730 MPa; (b) Specimen BF-54: $\bar{\sigma}_r$ = 400 MPa, max P = 905 MPa.....	16

List of Figures (Cont'd)

	Page
Figure 11. Angular particles in the vicinity of the shear plane for Starphire specimens tested with hydraulic confinement. (a) Specimen SP-10: $\bar{\sigma}_r = 250$ MPa, max $P = 710$ MPa; (b) Specimen SP-44: $\bar{\sigma}_r = 500$ MPa, max $P = 1100$ MPa.	17
Figure 12. Compacted particles in the vicinity of the shear plane for Specimen BF-83, tested quasistatically with mechanical confinement and a maximum confining pressure of 395 MPa, Five load/unload cycles were applied (Max $\sigma_{eq} = 2120$ MPa, Max $P = 1100$ MPa).	17
Figure 13. Compacted and sintered regions in Specimen BF-31 following compression testing (strain rate = 2 s^{-1} , 1 cycle only) with mechanical confinement. The micrograph on the right is a magnified view of Figure 13a.	18
Figure 14. Borofloat specimen (BF-16, $\bar{\sigma}_r = 100$ MPa) following testing with mechanical confinement. This pre-damaged specimen underwent a thermal shock treatment and ten load/reload cycles during compression testing.	19

List of Tables

	Page
Table 1. Approximate Composition of Borofloat [®] and Starphire [®] Glass [24].....	3
Table 2. Properties of Borofloat [®] and Starphire [®] Glass [24]	3

UNCLASSIFIED



1.0 Introduction

The strength of glass and other brittle materials increases with pressure. This pressure dependency is well documented for various materials, ranging from ceramics [1] to geologic materials [2]. The response of glass to a projectile/penetrator impact requires understanding of glass response under high pressure and shear stress. Although this topic has been the subject of numerous recent publications [3,4,5,6,7], improved understanding of the damage development process is necessary to aid with development of more accurate constitutive models. Such models can then be applied in design efforts to enhance ballistic performance through material and geometric arrangement of armor elements. Further insight into the pressure-dependent response of glass is critical for more effective design and development of transparent armor systems.

SwRI has investigated the effects of pressure/shear in the laboratory using non-ballistic experiments. Compression experiments are performed on confined specimens using either hydraulic confinement or mechanical confinement. Specimens are pre-damaged and then loaded and reloaded to comminute the material. This technique has been applied previously in our laboratory to evaluate the effects of pressure on the damage response of ceramics [8]. The experimental data obtained have been used to improve the Johnson-Holmquist constitutive model [9] for ceramics.

Other non-ballistic experiments have also been developed recently to improve understanding of the damage process and aid with modeling efforts. Shockey and colleagues [10,11] developed a test methodology to investigate the failure physics of projectile impact into thick (2-inch) borosilicate glass targets. They employed low-velocity ballistic experiments to evaluate the flow region under the penetrator and corresponding damage mechanisms. A new laboratory compression/shear experiment was devised by Nie, et al. [12] to evaluate the dynamic failure of glass. A modified version of the split Hopkinson (Kolsky) bar is used to generate a shear stress component in cuboid test specimens oriented at different angles to the loading direction. Experimental results for borosilicate glass show that the equivalent stress at failure decreases as the shear component of the stress increases. Chen, et al. [13,14] also developed a Hopkinson bar technique that utilizes double pulse loading to better simulate an impact event for a brittle material (e.g. ceramics or glasses). The first pulse determines the dynamic response of the intact material and then crushes the specimen; the second pulse determines the dynamic compressive response of a damaged material with interlocking pieces. A ring-on-ring technique was used by Wereszczak, et al. [15] to investigate contact damage for soda-lime and borosilicate glasses. Similar experiments were implemented at high strain rates using a Hopkinson bar setup [16].

Post-test microscopy investigations have been applied to better understand the damage development process. Shockey [10,11] evaluated the flow region under the penetrator in impacted targets of borosilicate glass. Some melting was observed on glass adhered to the projectile. Bless [17] investigated multilayered glass targets following projectile impact and documented the damage regions in individual layers. Nie and Chen [14] studied the effects of temperature and confinement pressure on the dynamic response of damaged borosilicate glass. Dannemann [18,19] evaluated the progression of damage and the effects of increasing confinement pressure based on interrupted laboratory compression tests for specimens with mechanical confinement. The fragmentation process in ceramics, which may be applicable to glass, is discussed in an extensive review by Grady [20]. LaSalvia and colleagues [21,22] are actively investigating damage mechanisms in ceramic armor materials with emphasis on the comminuted zone underneath the projectile impact location.

The results of confined compression tests on Borofloat and Starphire glass demonstrate that damaged glass exhibits a cap in strength as the hydrostatic pressure is increased. The strength cap is strain rate independent [23]. The objective of the present work was to investigate the flow and failure behavior of glass under confinement. This includes investigation of failure along observed shear planes. Borofloat and Starphire glass specimens were tested in confined compression under quasistatic loading. Several tests were also performed at higher strain rates ($\sim 1 \text{ s}^{-1}$ to 1000 s^{-1}). Confinement sleeves/holders were removed following testing and specimens evaluated using optical and electron microscopy. This work expands on prior work by the authors [18,19] where the onset and extent of damage in Borofloat glass were evaluated.

2.0 Materials

Borofloat[®]33 (BF) and Starphire[®] (SP) glasses were evaluated. Both glasses were obtained from Swift Glass, Elmira, NY. BF is a borosilicate glass manufactured by Schott Glass using a float process. SP float glass is a crystal clear, soda-lime glass. This low Fe, low Pb glass, manufactured by Pittsburgh Plate Glass (PPG), has a more consistent composition than ordinary soda-lime glass with similar physical and mechanical properties. Compositions of the two glasses are summarized in Table 1. These were determined from X-ray fluorescence analysis [24]. Both glasses also contain minor amounts of other oxides not included in the table (e.g., ZrO₂, BaO, SrO, Cr₂O₃). The high transparency of the BF and SP glasses, and the clear edge characteristics of the SP glass, is related to their low Fe content.

Table 1. Approximate Composition* of Borofloat[®] and Starphire[®] Glass [24]

Material	SiO ₂	Na ₂ O	CaO	B ₂ O ₃	Al ₂ O ₃	MgO	K ₂ O	Fe ₂ O ₃
Borofloat [®] 33	80.54	3.54	0.02	12.70	2.54	<0.01	0.64	0.015
Starphire [®]	73.23	14.71	10.28	--	1.45	0.08	0.01	0.008

* Values listed for each glass are normalized weight percentages, averaged from four separate analyses.

Properties of the BF and SP glasses were measured using an ultrasonic technique (ASTM E494[25]); the results are summarized in Table 2. The elastic modulus and Poisson's ratio determined from ultrasonic measurements are similar to those measured from the compression experiments. The density and Poisson's ratio are lower for BF vs. SP glass. The elastic and shear moduli are also lower for the BF glass. The linear coefficient of thermal expansion for each glass is also included for comparison purposes. These values were obtained from the manufacturer technical datasheets [26,27], not from ultrasonic measurements. The thermal expansion coefficient for BF glass is approximately one third the value for SP. The effect of this difference on the damage/crack pattern developed during the thermal shock procedure for pre-damaging the specimens is discussed subsequently.

Table 2. Properties of Borofloat[®] and Starphire[®] Glass [24]

	Borofloat [®] 33	Starphire [®]
Density (g/cc)	2.23	2.50
Elastic Modulus (GPa)	62.2	72.1
Shear Modulus (GPa)	26.0	29.5
Poisson's Ratio	0.195	0.222
Longitudinal Sound Speed, c _L (m/s)	5550	5750
Shear Wave Speed, c _S (m/s)	3416	3440
Linear Coefficient of Thermal Expansion*, α _L (°C ⁻¹)	3.25 x 10 ⁻⁶ [26]	9.28 x 10 ⁻⁶ [27]

* from 20°C to 300°C

Ceramic anvils, positioned between the test specimen and the loading platens, were used to load the confined specimens during compression testing. Initial tests were performed with tapered tungsten carbide (WC) loading anvils. Subsequent confined sleeve tests utilized higher strength SiC-N anvils, machined and processed by BAE Advanced Ceramics Division. Tapered alumina (AD-995) anvils were used for the hydraulic confinement experiments. The annular confining sleeves for the mechanical confinement tests were fabricated from maraging steel, Vascomax C350, to maximize confinement pressure without yielding the confining sleeve.

UNCLASSIFIED



3.0 Experimental Procedure

3.1 Specimen Preparation

The compression experiments were performed on polished cylindrical glass test specimens with a length to diameter (L/D) ratio of 2. The specimens were ground from plate by Swift Glass, and measured 6.35-mm in diameter and 12.7-mm long. Owing to the inherent flaw sensitivity of glass, all specimens were polished to a high-end optical finish (80/50 scratch-dig) to minimize surface defects. Flatness and parallelism of the specimen ends, especially critical when testing brittle materials, were maintained to within 0.005-mm.

Both intact and pre-damaged specimens were evaluated. Test specimens were pre-damaged using a thermal shock technique. The thermal shock procedure consisted of two 0.3-h exposures at 500°C in a resistance tube furnace, followed by an ice water quench after each thermal exposure. The procedure was applied to individual test specimens, rather than exposing multiple specimens at once. The thermal shock treatment was sufficient to pre-damage the glass specimens while maintaining specimen integrity so that specimens could be handled during test preparations without imparting further damage. Stereomicroscopy evaluations of the thermally shocked samples were performed prior to confinement testing to evaluate the extent of damage. A consistent damage pattern was observed for both types of glass specimens. Representative damage patterns are illustrated in Figure 1 and Figure 2 for the BF and SP glass, respectively.

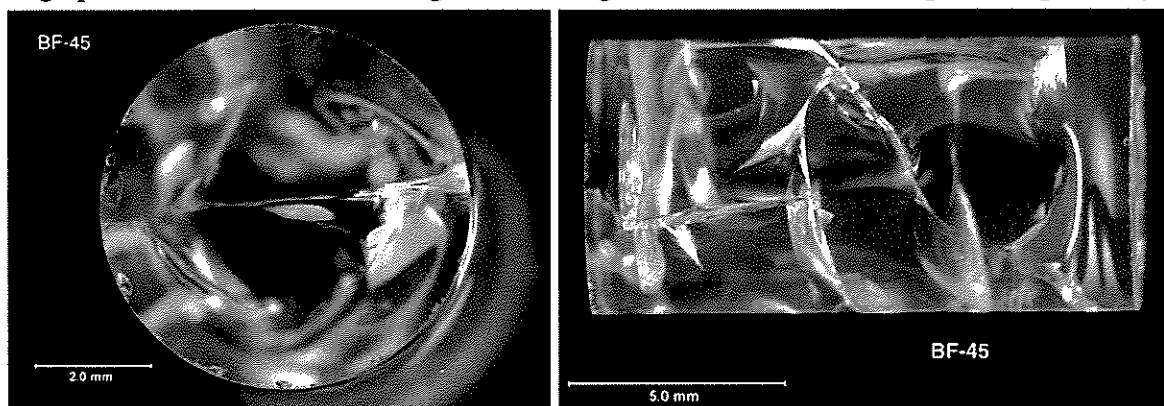


Figure 1. Pre-damaged Borofloat specimen (BF-45 end and side view) following a thermal shock treatment. The crack pattern is representative of the pre-damaged BF specimens.

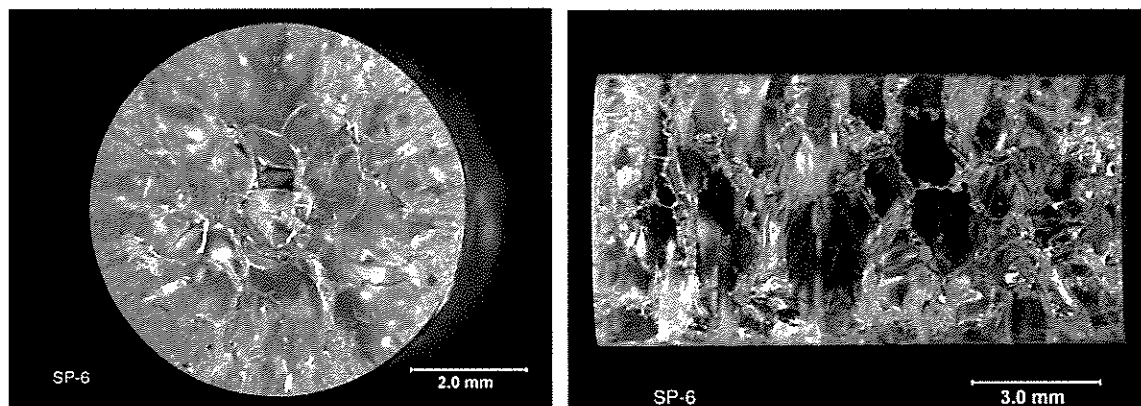


Figure 2. Pre-damaged Starphire specimen (SP-6) showing representative damage pattern for the Starphire glass specimens following the thermal shock procedure.

The damage pattern for the BF glass (Figure 1) shows a limited number of very distinct cracks. For SP glass (Figure 2), the thermal shock procedure produced a network of interconnected cracks. The damage pattern and extent differs from the BF specimens, though a similar thermal shock procedure was employed. This can be attributed to the higher thermal expansion coefficient (3x BF glass), as well as the low thermal shock resistance of SP glass.

3.2 Confined Compression Tests

Most compression experiments were conducted at quasistatic strain rates ($\sim 10^{-3} \text{ s}^{-1}$). Several tests were also performed at higher strain rates to assess strain rate dependence. These were conducted on pre-damaged specimens using a Hopkinson (Kolsky) bar setup. The quasistatic and intermediate rate ($\sim 1 \text{ s}^{-1}$) tests were conducted using an MTS servohydraulic machine. Specimens were confined using either a mechanical or hydraulic confinement technique.

With the hydraulic confinement technique, a constant confinement pressure is maintained during testing. The hydraulic confinement test is a triaxial compression test. This type of test is commonly used to characterize pressure-dependent materials (e.g., sand or concrete) [2,28]. A maximum confinement pressure of 500 MPa is possible with our current setup. Tests were performed at fluid pressures of 25, 50, 100, 250, 400, and 500 MPa. The glass specimens are placed in a Teflon shrink tube sleeve for protection from the hydraulic fluid. A piston is used to load the specimen inside the pressure vessel using two ceramic anvils. The load is measured with a load cell placed inside the pressure vessel and wired directly to provide the equivalent stress acting on the specimen. The axial strain in the specimen is measured using a calibrated extensometer.

For mechanical confinement, a 3.2-mm thick high-strength steel sleeve is used to confine the specimen during testing. Individual confining sleeves were honed to fit a specific test specimen. This minimized the clearance between the test specimen and the inner wall of the confining sleeve. The sleeved specimens were loaded (with ceramic anvils on the specimen ends) in displacement control. The confinement pressure changes during loading of the sleeved specimen. The maximum confining pressure depends on the extent of compressive loading; the maximum confining pressure achieved was approximately 1 GPa. Load is measured with the load cell on the MTS loadframe. Axial strains in the specimen were measured with an extensometer, with arms situated on the loading platens. Strain gages, mounted on the mid-section of the confining sleeve, were also used to measure axial and hoop strains in the sleeve. Additional details for the confined compression experiments and techniques are described in Refs. [8,18,23].

3.3 Post-Test Specimen Evaluation

Careful specimen preparation and handling was required to ensure the fracture/failure characteristics were captured without imparting further damage to the specimens, or disrupting loose or interlocking glass fragments. Specimens were evaluated to determine the extent of damage, with increasing load and pressure levels, and the extent of failure.

Initial investigations were performed with optical and stereomicroscopy; the damage was photo documented. Higher resolution microscopy, using a scanning electron microscope (SEM), was performed on select BF and SP specimens with damage features of interest. These were selected based on the optical microscopy evaluations. The SEM investigations were implemented to provide more detailed analyses in the vicinity of the dominant shear plane,

including the morphology of the glass fragments along the resulting shear plane. SEM evaluations required application of a gold coating to the glass specimens to limit specimen charging under the electron beam.

To view the damage *in-situ*, it was necessary to remove the steel sleeve or Teflon holder around the specimen. The technique for removing a section of the steel confinement sleeve was perfected in previous investigations [18]. A longitudinal section of the steel sleeve was carefully removed to minimize disturbance to the tested specimen. Removal of a “pie section” from the steel sleeve, as shown in Figure 3a, allowed viewing of *in-situ* damage along the entire specimen length. Internal damage was readily visible owing to the transparency of the glass. Cutting of the steel sleeve was initially performed with a Dremel tool; electro-discharge machining (EDM) was implemented subsequently to obtain precision cuts with minimal specimen damage. Numerous confined sleeve specimens were evaluated, as the location of the opening did not always correspond with the dominant shear plane location.

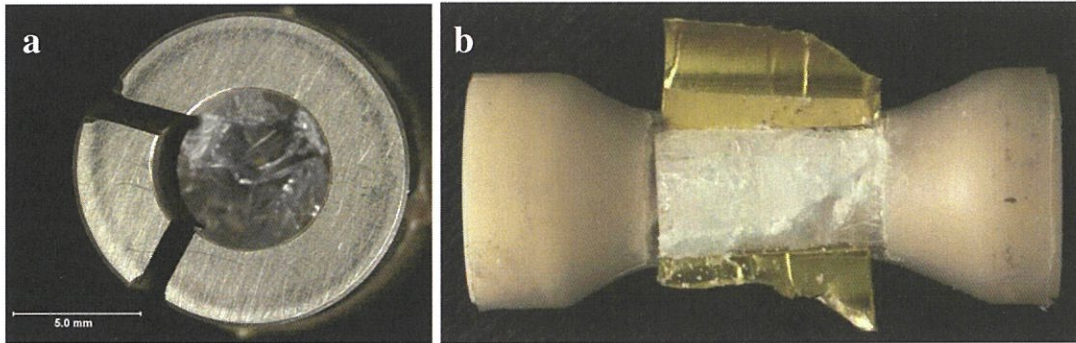


Figure 3. Removal of the confining sleeve/holder was necessary to view *in-situ* damage following compression testing of. (a) Confined sleeve specimen – end view (b) Triaxial compression specimens (B52_3) – lengthwise view.

For specimens tested in triaxial compression, slitting and opening of the Teflon sleeve, and underlying brass foil, was necessary to view specimen damage. The thin brass foil was wrapped around the specimen to prevent damage to the Teflon shrink tubing due to fragmentation of the glass during testing. Perfection of the cutting/opening technique was required to minimize further damage to the specimen. If the position of the anvils within the Teflon sleeve was not maintained during the sectioning process, shifting and disruption of glass fragments along the shear plane occurred. Figure 3b shows a BF specimen tested in triaxial compression following cutting and opening of the shrink tube.

UNCLASSIFIED



UNCLASSIFIED

4.0 Results

Axial stress vs. axial strain curves were obtained for each confined compression test. For the confined sleeve tests, axial stress vs. hoop strain plots were also obtained. The axial stress-strain response of intact and pre-damaged BF and SP glass are compared in Figure 4 for specimens tested with hydraulic confinement; confinement pressures are included on the plot. Each curve corresponds to a single test, and is representative of the behavior of each glass at similar confinement pressures. The response differs for intact vs. predamaged glass, but is consistent for BF and SP glass.

The axial stress-strain curves for *intact* confined glass follow a similar trajectory. The failure stress for the intact glass increases with confining pressure. The stress-strain curves for the intact glasses are generally linear until failure. Failure occurs suddenly and is indicated by the vertical arrows in Figure 4. Some deviation from linearity is evident for the intact BF glass. The cause of the non-linearity was not investigated, but may be related to densification of the glass. Densification of BF glass has been demonstrated in recent work by Holmquist and Johnson [3].

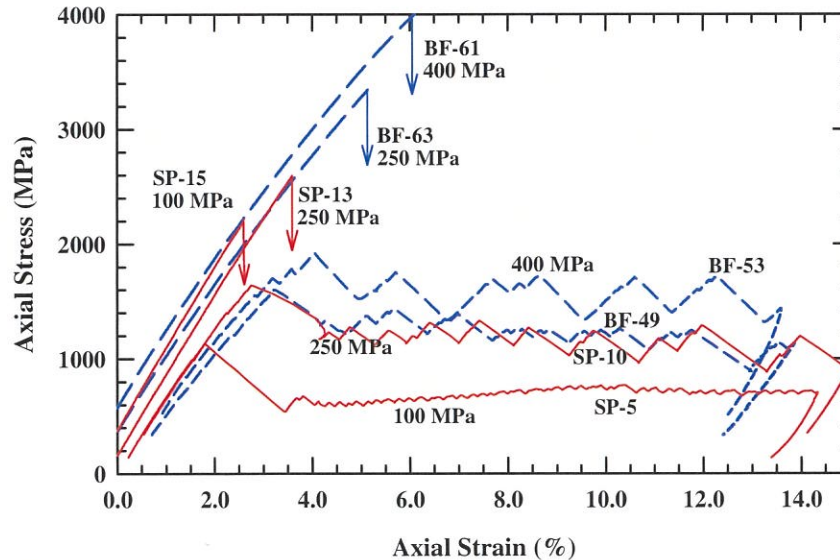


Figure 4. Axial stress-strain response of intact and pre-damaged Borofloat (blue curves) and Starphire (red curves) specimens tested in triaxial compression.

The *predamaged* glass exhibits a dramatic response difference vs. the intact specimens. A linear stress-strain response was measured upon initial loading of the confined, predamaged specimens. The moduli are less than for the corresponding intact specimens, owing to the presence of cracks in the predamaged specimens. With continued loading, a maximum axial stress is reached; this stress is lower than the failure strength of the corresponding intact glass. The strength then drops to a lower value which is maintained with increasing axial strain, as shown in Figure 4. This indicates load carrying capability even after initial damage occurs. Previous interrupted tests on BF glass specimens with mechanical confinement (steel sleeve) showed specimen strength was maintained until a critical stress level was exceeded [19]. The residual strength values shown in Figure 4 vary with the confinement pressure; higher confining pressure corresponds to higher residual strength. Similar residual strengths were measured for BF and SP glass at each confinement pressure tested. The fluctuation in the curves around the

residual strength value likely occurs due to particle movement and extension of pre-existing cracks. This is discussed in more detail in the next section of this report. Additional details on the mechanical response are provided in previous reports [29,30].

Experimental data from both types of tests were reduced to equivalent stress versus pressure plots for direct performance comparisons of the two glasses, and to assess the effect of specimen condition (e.g., intact, pre-damaged, etc.) on response. The equivalent stress, for axial symmetry, is defined by:

$$\sigma_{eq} = |\sigma_z - \sigma_r| = \tilde{\sigma}_z - \tilde{\sigma}_r \quad (1)$$

where σ_z is the axial load and σ_r is the radial load. For the triaxial compression tests, σ_r is the fluid pressure from the hydraulic confinement ($\sigma < 0$ in compression, $\tilde{\sigma} > 0$ in compression). For the confined sleeve tests, σ_r is determined analytically based on the hoop strain in the steel sleeve – assuming the sleeve remains elastic [23]. The pressure for the equivalent stress vs. pressure plots is the hydrostatic pressure derived from the confining pressure. The hydrostatic pressure on the specimen is given by Eqn (2). See Chocron, et al. [23] for details of the analysis.

$$P = \frac{1}{3}(2\tilde{\sigma}_r + \tilde{\sigma}_z) \quad (2)$$

Maximum equivalent stress vs. hydrostatic pressure comparison plots for intact and pre-damaged glass are shown in Figure 5 and Figure 6, respectively. The behavior of confined vs. unconfined *intact* glass is compared in Figure 5 for BF and SP glass. The equivalent stress versus pressure response for *intact*, unconfined glass lies on a line with a slope of 3, from Eqn. (1) and (2) since $\tilde{\sigma}_r = 0$ for the unconfined tests. There is considerable scatter in the intact strength of both glasses. On average, BF glass is stronger than SP glass. The strength (i.e., equivalent stress) increases with confinement. In general, as the confinement increases, the scatter in the intact strength decreases.

The confined compression test results for *pre-damaged* BF and SP glasses are shown in Figure 6. Both predamaged glasses exhibit similar behavior at hydrostatic pressures less than ~1 GPa; the predamaged data in Figure 4 are in this pressure range. When the hydrostatic pressure exceeds a critical pressure, a strength cap occurs. Pre-damaged SP glass exhibits a strength cap at approximately 1.6 GPa. The strength of the pre-damaged BF glass continues to increase until reaching an approximate equivalent stress of 2.1 GPa. Figure 6 shows the strength cap is approximately 0.5 GPa higher for BF glass. The residual strength difference between the BF and SG glass may help to explain recent findings by Bless [31] where BF glass demonstrated greater penetration resistance vs. SP glass in depth of penetration experiments using both blunt and sharp projectiles.

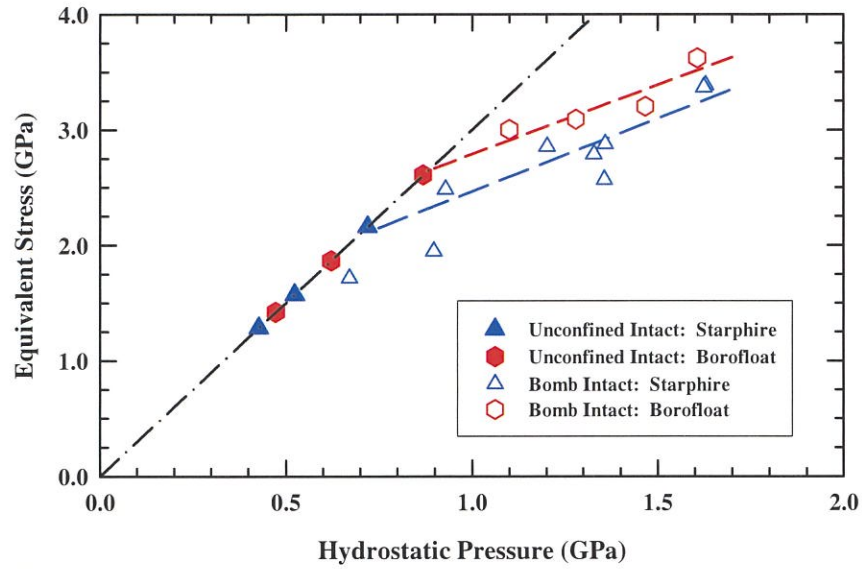


Figure 5. Equivalent stress vs. hydrostatic pressure comparison plot for intact Borofloat and Starphire glass specimens for data obtained from confined (bomb intact) and unconfined tests [32].

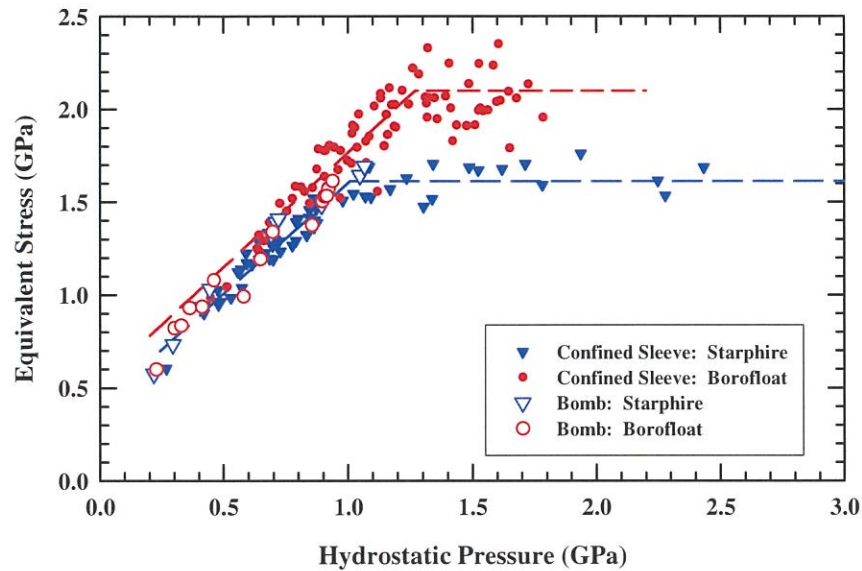


Figure 6. Equivalent stress vs. hydrostatic pressure comparison plot obtained from confined compression test data on pre-damaged Borofloat and Starphire glass specimens [32].

UNCLASSIFIED



UNCLASSIFIED

5.0 Discussion

The slopes of the equivalent stress vs. pressure plots in Figure 5 and Figure 6 are independent of the damage condition (i.e., intact vs. predamaged). However, the intercept varies with the extent of damage. The lower residual strength of predamaged SP glass (vs. predamaged BF glass), shown in Figure 6, may be related to the higher level of initial damage for SP glass. See Figure 1 and Figure 2 for a comparison of the predamage condition. SP glass exhibits a network of interconnected cracks following thermal shock. The initial damage was more extensive than for BF glass although the same thermal shock procedure was applied. The lower thermal shock resistance and more extensive cracking exhibited by the SP glass can be related to the difference in linear expansion coefficient (3x greater for SP glass vs. BF glass).

The difference in response for the unconfined intact glasses, shown in Figure 5, demonstrates an inherent compositional difference between SP and BF glass. Compositional differences (see Figure 6) may also indirectly affect the maximum strength (cap) of the predamaged glass. The strengths of the predamaged glasses are similar at lower pressures. The difference becomes more pronounced at higher pressures: greater than 1.0 GPa and 1.2 GPa for SP and BF glass, respectively.

Axial loading of both glasses, whether intact or pre-damaged, results in formation of a dominant shear plane. Damage likely initiates from flaws and/or pre-existing cracks due to the thermal shock procedure. Compression loading of the specimen causes slippage, and movement of the material. For BF glass, specimens exhibited "slip" along a shear plane located at a 55°- 70° angle from the compression loading axis. The shear angle for the SP specimens was slightly less, with an orientation of 50°- 60° from the loading axis. Figure 7 shows the shear planes observed for specimens tested with hydraulic confinement (for confining pressures up to 400 MPa). The shear plane becomes more pronounced with increased confinement pressure.

Shear planes were also observed for confined sleeve specimens tested to higher confining pressures. The maximum confinement pressure achieved for the sleeve tests was approximately 1 GPa. The sectioned BF and SP specimens shown in Figure 8 are representative of the findings for the confined sleeve tests. Note the dominant shear plane marked by the red arrows, and the similarity in the shear angle for these tests vs. the triaxial compression test results in Figure 7. The maximum confining pressure for these test specimens was 870 and 770 MPa for the BF and SP glasses, respectively. These observations indicate that the orientation of the shear failure is (i) independent of the confinement method (i.e., hydraulic vs. mechanical confinement), and (ii) independent of the confinement pressure for both glasses. It also appears independent of strain rate, based on limited high strain rate ($\sim 1 \text{ s}^{-1}$, $\sim 1400 \text{ s}^{-1}$) test results for these two glasses.

Post-test microscopy revealed internal damage, as well as surface damage. This was detected based on evaluation of several specimens at different viewing angles. Post-test evaluation of Specimen BF-37 (Figure 8a) showed that the specimen curvature was maintained without disruption of specimen fragments. Evaluation of several specimens that were gold coated for SEM evaluation showed the coated specimens appeared more intact than uncoated specimens. This is illustrated in Figure 9 for specimen SP-8 following triaxial compression testing (confinement pressure = 100 MPa). The gold coating reduces the transparency of the glass, highlighting cracks that originate from or extend to the surface. Without the gold coating, it cannot be determined whether the damage occurs on the surface or is interior to the glass (Figure 9a).

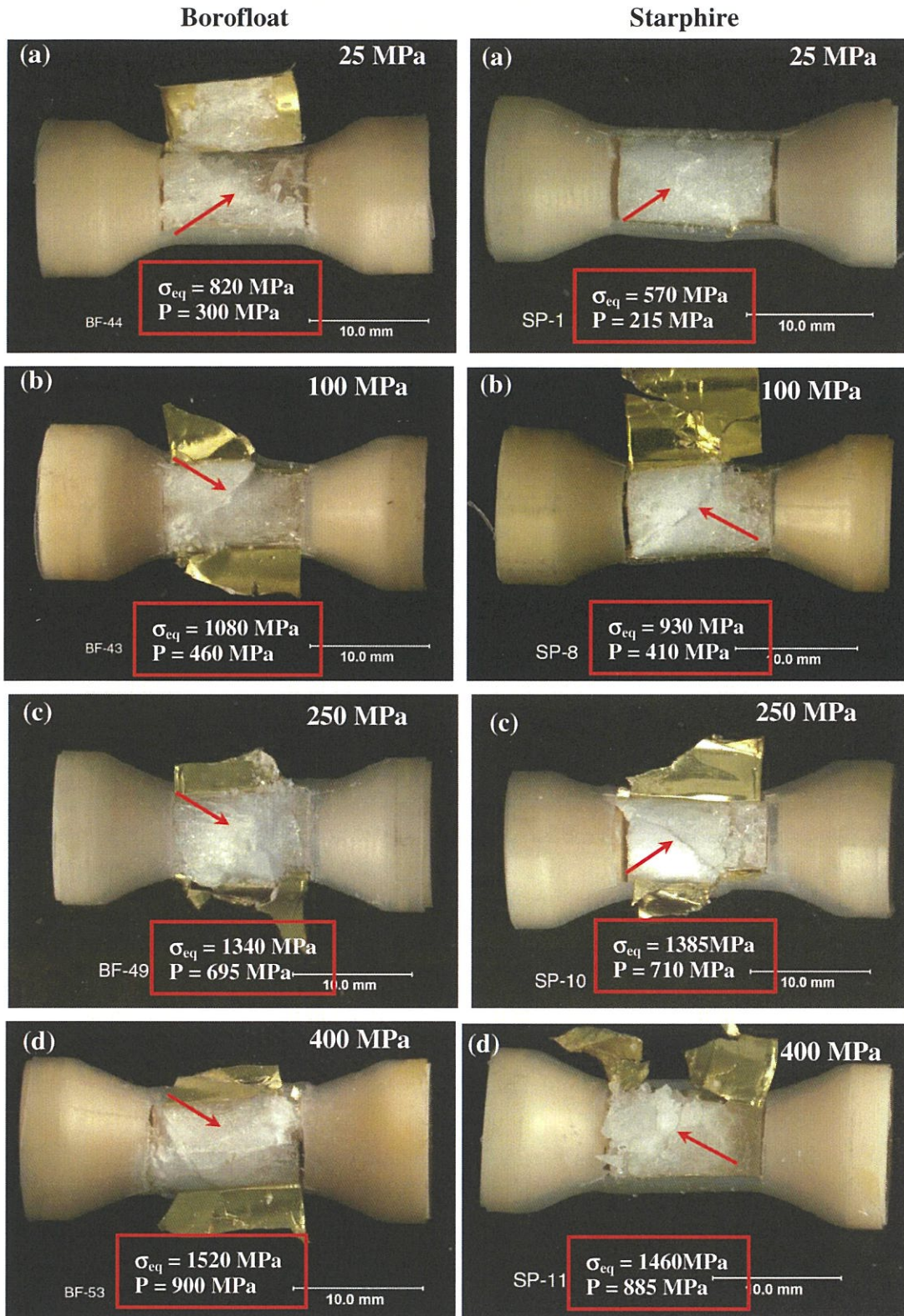


Figure 7. Pre-damaged Borofloat and Starphire specimens following monotonic loading with hydraulic confining pressures of (a) 25 MPa, (b) 100 MPa, (c) 250 MPa, (d) 400 MPa. The dominant shear plane is marked in each photograph. Orientation of the shear plane is 55-70° from the loading axis for Borofloat, and 50-60° for Starphire. The equivalent stress and hydrostatic pressure (in red box) correspond to the data plotted in Figure 6.

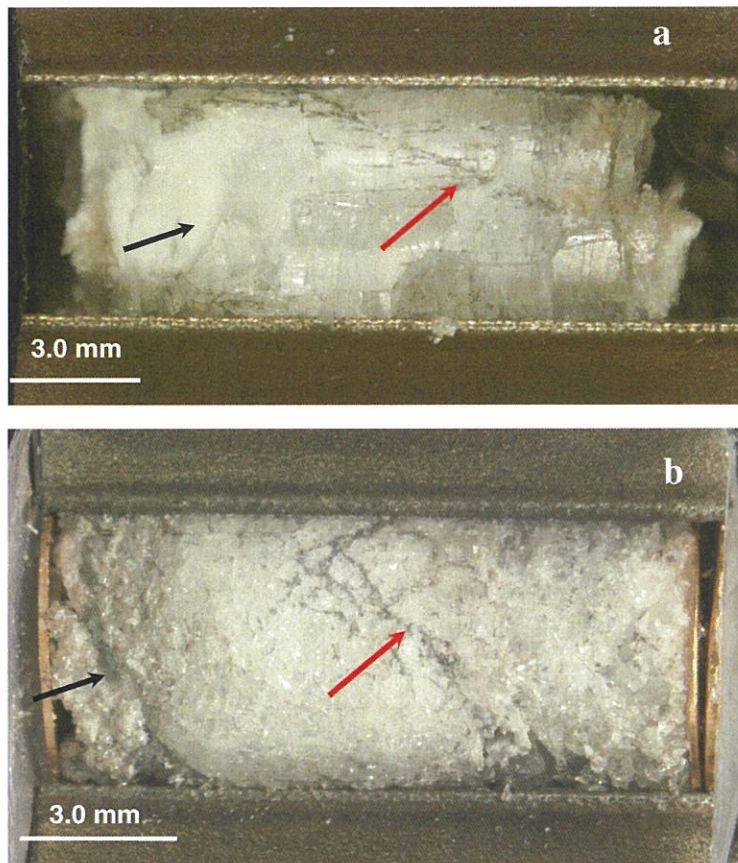


Figure 8. Dominant shear plane (red arrow) and secondary damage regions (black arrow) formed during confined sleeve testing of:
 a) Borofloat (BF-37): Max $\sigma_{eq} = 2210$ MPa, Max $\tilde{\sigma}_r = 870$ MPa; Max $P = 1580$ MPa.
 b) Starphire (SP-25): Max $\sigma_{eq} = 1700$ MPa, Max $\tilde{\sigma}_r = 770$ MPa; Max $P = 1300$ MPa.

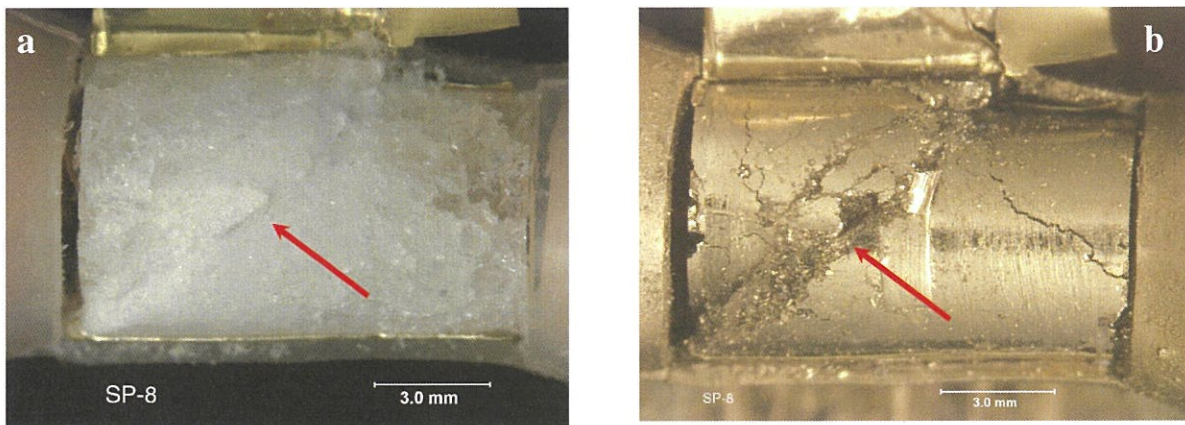


Figure 9. Starphire specimen (SP-8, $\tilde{\sigma}_r = 100$ MPa) following compression testing with hydraulic confinement: (a) as tested; (b) identical specimen following gold coating.

SEM evaluations provided detailed views of the damage in the vicinity of the dominant shear plane for select predamaged specimens following testing. For BF glass, a dusting of very fine ($< 1 \mu\text{m}$) particles was detected in the vicinity of the dominant shear plane. Fine particles are likely dislodged during axial loading as the specimen shifts to relieve the pressure. Higher magnification microscopy revealed the fine particles are actually aggregates of particles; few individual particles were observed. Generally, the aggregates were composed of rounded or spherical particles, as illustrated by the micrographs in Figure 10 for two representative BF specimens. Similar particle morphologies were also observed by Nie and Chen [14] in BF glass specimens following high strain rate compression tests conducted with a double pulse to simulate fracture and compaction. For BF specimens tested at a higher confining pressure, a hackle region was detected on some of the particles/aggregates. This is characteristic of brittle fracture, and is illustrated at two different locations (red arrows) in Figure 10b. The two different orientations of the hackle lines indicate crack branching likely occurred.

The SP specimens exhibited greater fragmentation than the BF specimens following confinement testing. Loose particles were also detected in the vicinity of the dominant shear plane in predamaged SP glass. However, these particles were generally large and angular, as shown in Figure 11. Fewer round particles were observed in SP glass. The shape and size of the SP particles (Figure 11) are easily compared with the BF particles (Figure 10); note the scale difference. The absence of very fine particulates in the SP glass is indicative of less comminution than the BF glass, possibly due to the high density of pre-existing cracks. Whiskers were detected in some SP specimens following compression testing; see red arrow in Figure 11b. These have also been reported by Bless [17] for soda-lime glass targets following high speed projectile impact. This phenomenon was not explored; further investigation is necessary to determine the growth kinetics.

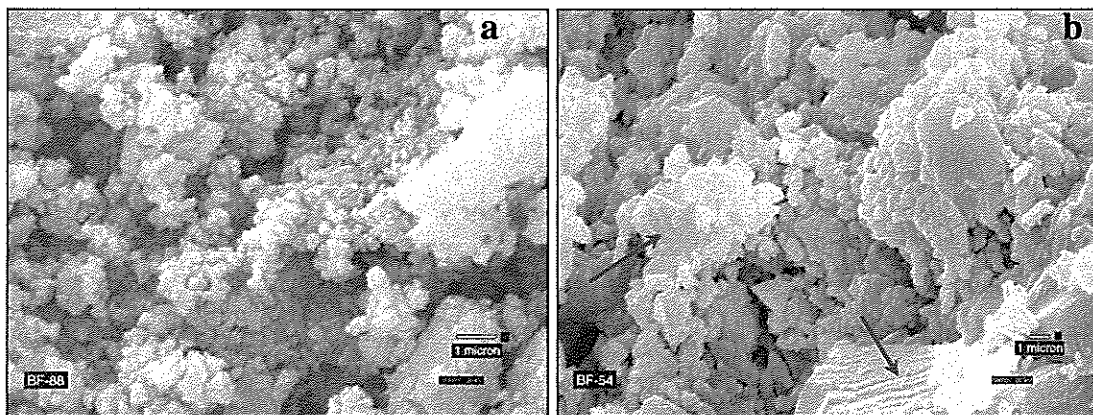


Figure 10. Rounded particles in the vicinity of the shear plane for Borofloat specimens tested with hydraulic confinement. (a) Specimen BF-88: $\bar{\sigma}_c = 250 \text{ MPa}$, $\text{max } P = 730 \text{ MPa}$;
(b) Specimen BF-54: $\bar{\sigma}_c = 400 \text{ MPa}$, $\text{max } P = 905 \text{ MPa}$.

Deformed and compacted glass particles were observed in the vicinity of the shear plane for some BF glass specimens, This is illustrated in Figure 12 for Specimen BF-83 following five compression load/reload cycles with mechanical confinement (max. confining pressure $\sim 395 \text{ MPa}$). The absence of loose particles and surface characteristics are evidence that particle sliding or rubbing occurred, resulting in compaction. A similar morphology was observed by Shockey, et al. [10,11] in the vicinity of the projectile following laboratory scale impact experiments on borosilicate glass. Further insight is provided upon examination of Figure 13.

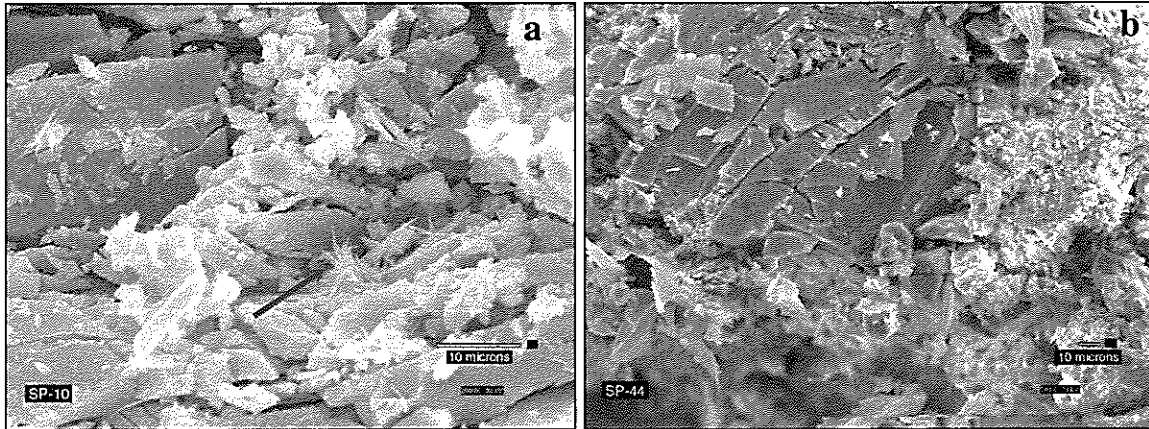


Figure 11. Angular particles in the vicinity of the shear plane for Starphire specimens tested with hydraulic confinement. (a) Specimen SP-10: $\bar{\sigma}_r = 250$ MPa, max $P = 710$ MPa; (b) Specimen SP-44: $\bar{\sigma}_r = 500$ MPa, max $P = 1100$ MPa.

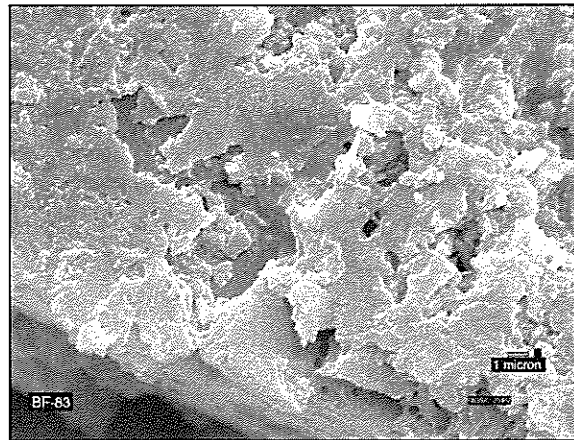


Figure 12. Compacted particles in the vicinity of the shear plane for Specimen BF-83, tested quasistatically with mechanical confinement and a maximum confining pressure of 395 MPa. Five load/unload cycles were applied (Max $\sigma_{eq} = 2120$ MPa, Max $P = 1100$ MPa).

For several of the BF specimens, it appears that the pressure was high enough for sintering of the particles to occur. This is illustrated in Figure 13 for a BF specimen tested with mechanical confinement at a strain rate of 2 s^{-1} ; the maximum hydrostatic pressure in the specimen approached 2.0 GPa. At lower magnifications, the compacted region appears as compacted particles, as shown in the SEM micrograph in Figure 13a. The compacted particles appear sintered, as shown in the magnified view in Figure 13b. Compacted regions were not observed for SP glass following similar testing. For SP glass, the pressure is relieved with extension of pre-existing cracks and shear plane formation.

Optical and SEM findings were compared to the mechanical response data, and used to support a hypothesis for the damage mechanism and continued load carrying capability of predamaged glass, as shown in Figure 4. Pressure buildup in the confined specimen, resulting from axial loading, causes movement and shifting within the glass specimen to relieve the pressure. This results in dislodgement of glass particles, as shown in Figure 10 and Figure 11 for BF and SP glass, respectively. Damage likely initiates at dominant flaws (e.g., pre-existing

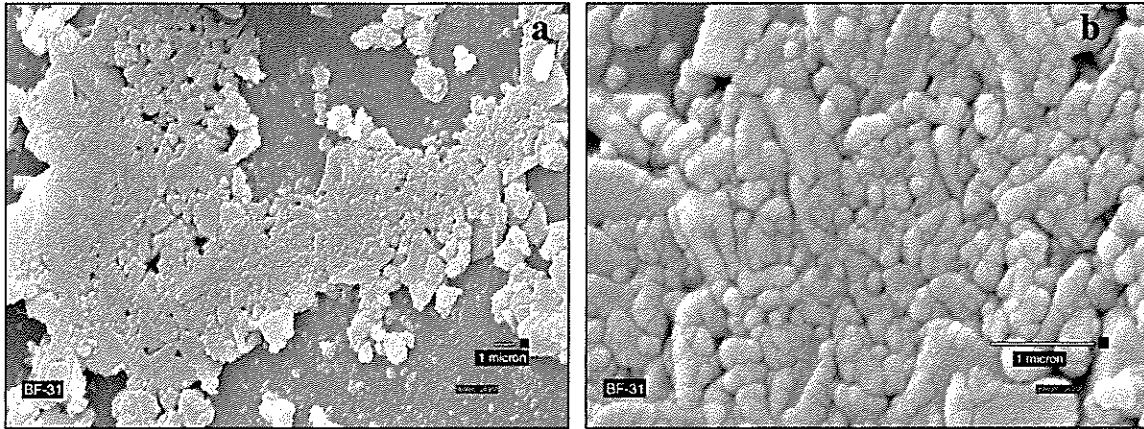


Figure 13. Compacted and sintered regions in Specimen BF-31 following compression testing (strain rate = 2 s^{-1} , 1 cycle only) with mechanical confinement. The micrograph on the right is a magnified view of Figure 13a.

$$\text{Max } \sigma_{eq} = 2200 \text{ MPa}, \bar{\sigma}_r = 1245 \text{ MPa}; \text{Max } P = 1980 \text{ MPa}$$

cracks due to the thermal shock treatment); propagation proceeds with continued loading. The different orientations of the hackle regions, shown in Figure 10b, imply that damage propagation proceeds in different planes and directions. Eventually, separate damage regions link together. Initial failure occurs by slippage along a dominant shear plane, as shown in Figure 7 and Figure 8, when the specimen can no longer support the maximum applied load. Subsequent loading of the confined specimen after formation of the dominant shear plane causes further shifting of the particles and fragments, and the creation of secondary damage regions and additional shear planes.

Shifting of the glass material during axial loading requires movement of particles within the confined specimen. As the axial load is increased, the particles attempt to slide over each other. This requires considerable activation energy, based on the observed particle morphologies (see Figure 10 and Figure 11). Initial movement is limited by frictional resistance between the particles. With continued loading, and increased axial stress, some particle sliding occurs. Movement becomes easier as particle compaction occurs and the particles are smoothed. Particle sintering, as shown in Figure 13, may occur with continued pressurization if high enough pressures are reached. Particle compaction and/or sintering result in decreased frictional resistance. Hence, the stress required for particle motion decreases. Sliding of adjacent surfaces occurs more readily. The compacted zones detected in the tested specimens (see Figure 12 and Figure 13) provide evidence for operation of this phenomenon. Frictional resistance, followed by easy sliding of the particles past each other, likely accounts for the stress variations observed in the axial stress-strain curves in Figure 4. When the particle surfaces have been sufficiently smoothed due to sliding, this mechanism disappears and a constant stress level is maintained.

At the outset of this section, the residual strength difference, shown in Figure 6, was indirectly attributed to compositional differences between the two glasses. The 0.5 GPa strength difference is rather large considering that the predamaged glasses demonstrate similar performance at hydrostatic pressures less than 1 GPa. The SEM post-test evaluations highlighted differences in the morphology of the particles. The inherent difference in the resultant particle shape following deformation is related to the specific glass composition. However, the extent of particle movement and sliding also contributes to the mechanical response. It is thought that this

mechanical phenomenon also contributes to the observed difference in the strength cap. Material movement occurs more readily in SP glass owing to the angular, but plate-like particles. Confinement keeps the cracks from opening so that the angular particles cannot orient randomly. Rather, there is a tendency for the plate-like particles to stay oriented for preferential sliding. Sliding and shifting of particles is more restricted in BF glass owing to the spherical shape of the particles and larger size of the aggregates, observed in the vicinity of the shear plane in the BF specimens evaluated.

Further evidence of the results of the high pressures experienced during loading (of select specimens) is illustrated by strong adherence of damaged glass regions to the steel confining sleeve and to the underlying brass foil for specimens tested in triaxial compression. Figure 7a illustrates this phenomenon for a specimen tested with hydraulic confinement. The glass particles strongly adhere to the brass foil and were not easily loosened. Energy dispersive spectroscopy (EDS) of a steel confining sleeve without adhered glass showed high levels of Si and O on the sleeve, indicating that the Borofloat glass specimens were pushed into the confining sleeve due to the high pressures during testing.

Continued loading of the confined glass specimens results in secondary damage regions, removed from the dominant shear plane. These regions are characterized by additional cracking and fragmentation, and were detected in both glasses. Primary and secondary damage regions are shown in Figure 8 for Specimens BF-37 and SP-25. The dominant shear plane is marked by the red arrow; the black arrows highlight the secondary damage regions. Secondary damage regions were more prevalent in specimens tested at higher confining pressures.

Damage was more extensive for glass specimens that were exposed to multiple load cycles. For the triaxial tests, load cycling was performed after the thermal shock procedure to "comminute" the glass prior to testing. For some of the mechanical confinement tests at low strain rates, specimens were exposed to multiple load cycles. An increase in the extent of specimen damage with load cycling was first confirmed for BF glass based on a series of interrupted tests with increasing number of load cycles and load magnitude [18,19]. An increase in the number of shear planes formed due to multiple load cycling was detected in recent evaluations. These are illustrated in Figure 14 for a BF specimen following ten load/reload cycles with mechanical confinement. The dominant shear plane is highlighted by the red arrow; the other shear planes are marked with black arrows.

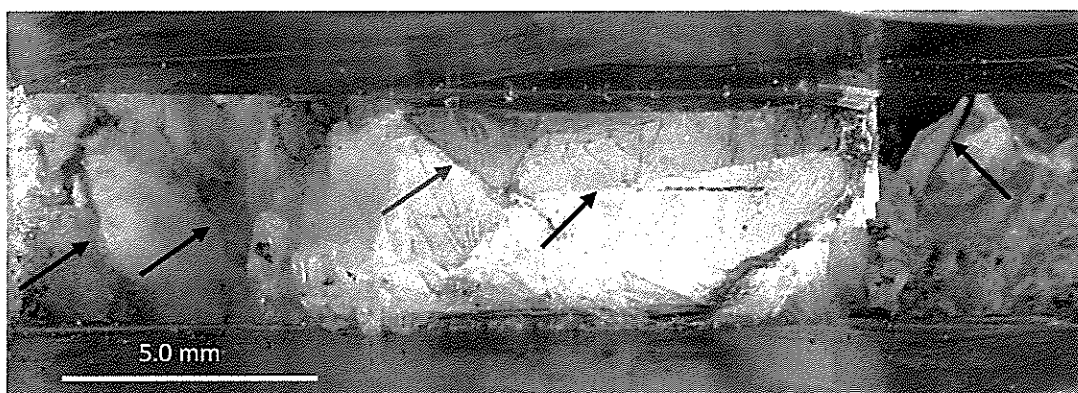


Figure 14. Borofloat specimen (BF-16, $\bar{\sigma}_c = 100$ MPa) following testing with mechanical confinement. This pre-damaged specimen underwent a thermal shock treatment and ten load/reload cycles during compression testing.

UNCLASSIFIED



UNCLASSIFIED

6.0 Summary

Compression test results with confinement showed very different behavior for intact vs. predamaged Borofloat (BF) and Starphire (SP) glass. Both *intact* glasses failed suddenly upon loading. Observed variability in failure stress and strain of the intact glass is attributed to flaw sensitivity in these materials. *Predamaged* glass, both BF and SP, exhibited a linear axial stress-strain response with initial loading, though the moduli were less than the corresponding intact glass. Both predamaged glasses exhibited a drop in strength after initial failure, but maintained a load carrying capability. The residual strength (i.e., strength cap) is approximately 2.1 GPa and 1.6 GPa for BF and SP glasses, respectively.

Post-test microscopy evaluations were conducted to assess the damage development process that occurs during confined compression loading of intact and pre-damaged Borofloat and Starphire glass specimens. Optical and electron microscopy findings were compared to the mechanical response data, and used to support a hypothesis for the damage mechanism.

The damage development process likely progresses from dislodgement of glass particles in the confined specimens to shifting/movement of glass particles and overcoming frictional resistance. The observed differences in particle morphology between the two glasses are attributed to compositional differences. The extent of particle movement and sliding likely contributes to the stress variations in the axial stress-strain curve and the observed difference in the strength cap of the two glasses.

Damage initiates at dominant flaws (e.g., pre-existing cracks due to the thermal shock treatment). Damage propagation proceeds with continued loading with resultant linkage of the damage regions. Initial failure occurs by slippage along a dominant shear plane when the specimen can no longer support the maximum applied load. The orientation of the shear plane differed slightly for the two glasses: 55°-70° angle for BF vs. 50°-60° for SP. This orientation occurred independent of the confinement pressure and strain rate.

Subsequent loading of the confined specimen after formation of the dominant shear plane causes further shifting of the particles and fragments, and the creation of secondary damage regions and additional shear planes.

UNCLASSIFIED



UNCLASSIFIED

7.0 Acknowledgements

The authors gratefully acknowledge the financial support of the US Army (Contract W56HZV-06-C-0194) for this work. Dr. Doug Templeton and Mr. Rick Rickert of TARDEC are acknowledged for their technical and administrative support. Appreciation is also extended to Mr. Parimel Patel (US Army Research Laboratory) for providing the glass specimens tested early in this program, and for ultrasonic measurements on both glasses. Mr. Art Nicholls (SwRI) is acknowledged for his skillful assistance with predamaging the test specimens, and confined compression testing.

UNCLASSIFIED



UNCLASSIFIED

8.0 References

1. J.Lankford, C.E. Anderson, Jr., A.J. Nagy, J.D. Walker, A.E. Nicholls, R.A. Page, "Inelastic Response of Confined Aluminum Oxide under Dynamic Loading Conditions", *J. Materials Science*, **33**(6): 1619–1625, 1998.
2. S.C. Desai and H.J. Siriwardane, *Constitutive Laws for Engineering Materials with Emphasis on Geologic Materials*, Prentice-Hall, Englewood Cliffs, NJ, 1984.
3. T. J. Holmquist, G.R. Johnson, "A Computational Constitutive Model for Glass Subjected to Large Strains, High Strain Rates and High Pressures", *J. Appl. Mech.*, in publication, 2011.
4. D.R. Curran, D.A. Shockey and J.W. Simons, "Mesomechanical Constitutive Relations for Glass and Ceramic Armor", in *Advances in Ceramic Armor IV*, Ceramic Engineering and Science Proc., *32nd Int. Conf. on Advanced Ceramics and Composites*, edited by L. Prokurat-Franks, **29**(6): 3-13, Wiley, 2008.
5. D. Curran, "Mesomechanical Modeling of Fracture", *Shock Compression of Condensed Matter – 2009*, edited by M.L. Elert, W.T. Buttler, M.D. Furnish, W.W. Anderson and W.G. Proud, CP1195, AIP, pp 3-10, 2009.
6. C. Lai, X Sun, and D.W. Templeton, "Analyses of Various Damage Mechanisms in Transparent Armor Subject to Projectile Impact", in *Advances in Ceramic Armor V*, *Proc. of the 33rd Int. Conf. on Advanced Ceramics and Composites*, edited by J.J. Swab, **30**(5): 205-212, Wiley, 2009.
7. P. Forquin and F. Hild, "A Probabilistic Damage Model of the Dynamic Fragmentation Process in Brittle Materials", *Advances in Applied Mechanics*, **44**: 1-72, 2010.
8. K. A. Dannemann, S. Chocron, A. E. Nicholls, J. D. Walker, and C. E. Anderson, Jr., "Compression testing and response of SiC-N ceramics: Intact, damaged and powder," *Advances in Ceramic Armor*, Ceramic Engineering and Science, *Proc.*, *29th Int. Conf. on Advanced Ceramics and Composites*, edited by J.J. Swab, **26**(7): 109-116; Wiley, 2005.
9. T.J. Holmquist and G.R. Johnson, "The Failed Strength of Ceramics Subjected to High-Velocity Impact", *J. Appl. Physics*, **104**, 013533, 2008.
10. D.A. Shockey, J.W. Simons, and D.R. Curran, "The Damage Mechanism Route to Better Armor Materials", *Int. J. Appl. Ceram. Technol.*, **7**(5): 566–573, 2010.
11. D. A. Shockey, D. Bergmannshoff, D. R. Curran, and J. W. Simons "Physics of Glass Failure during Rod Penetration," *Advances in Ceramic Armor IV*, Ceramic Engineering and Science Proc., *32nd Int. Conf. on Advanced Ceramics and Composites*, edited by L. Prokurat-Franks, **29**(6): 23-32, Wiley, 2008.
12. X. Nie, W.W. Chen, X. Sun, D.W. Templeton, "Dynamic Failure of Borosilicate Glass Under Compression/Shear Loading Experiments", *J. Am. Ceram. Soc.*, **90**(8): 2556–2562, 2007.
13. H. Luo and W. Chen, "Dynamic Compressive Response of Intact and Damaged AD995 Alumina", *Int. J. Appl. Ceram. Technol.*, **1**(3): 254–269, 2004.

14. X. Nie and W. Chen, "Temperature and Confinement Pressure Effects on Dynamic Response of Damaged Borosilicate Glass", American Ceramic Society, *35th Int. Conf. on Advanced Ceramics and Composites*, Daytona Beach, FL 2011.
15. A. A. Wereszczak, K. E. Johanns, T. P. Kirkland, C. E. Anderson Jr., T. Behner, P. Patel, and D. Templeton, "Strength and Contact Damage Responses in a Soda-Lime-Silicate and a Borosilicate Glass"; Paper FP-05, *25th Army Science Conference*, Orlando, FL, November 27-30, 2006.
16. X. Nie, W. Chen., A.A. Wereszczak., D.W. Templeton, "Effects of Loading Rates and Surface Conditions on Flexural Strength of Borosilicate Glass", *J. Am. Ceram. Soc.*, **92**(6): 1287-1295, 2009.
17. S. Bless and T. Chen, "Impact Damage in Layered Glass", *Int. J. Fracture*, **162**(1-2): 151-158, 2010.
18. K. A. Dannemann, A.E. Nicholls, C.E. Anderson, Jr., S.Chocron, J.D. Walker, "Response and Characterization of Confined Borosilicate Glass: Intact and Damaged", *Advances in Ceramic Armor II: Ceramic Engineering and Science Proceedings*, edited by A. Wereszczak, E. Lara-Curzio, L. Prokurat Franks, **27**(7): 119-130, Wiley, 2006.
19. K.A. Dannemann, S. Chocron, A.E. Nicholls and C.E. Anderson, Jr., "Compressive Damage Development in Confined Borosilicate Glass", *Materials Science and Engineering: A*, **478**: 340-350, 2008.
20. D.E. Grady, "Fragmentation of Ceramics in the Ballistic Environment", in *Advances in Ceramic Armor V, Proc. of the 33rd Int. Conf. on Advanced Ceramics and Composites*, edited by J.J. Swab, **30**(5): 3-17, Wiley, 2009.
21. J.C. LaSalvia and J.W. McCauley, "Inelastic Deformation Mechanisms and Damage in Structural Ceramics Subjected to High Velocity Impact", *Int. J. Appl. Ceram. Technol.*, **7**(5): 595-605, 2010.
22. J.C. LaSalvia, R.B. Leavy, J.R. Houskamp, H.T. Miller, D.E. MacKenzie and J. Campbell, "Ballistic Impact Damage Observations in a Hot-Pressed Boron Carbide", in *Advances in Ceramic Armor V, Proc. of the 33rd Int. Conf. on Ceramics and Advanced Composites*, **30**(5): 45-55, Wiley, 2009.
23. S. Chocron, C.E. Anderson, A.E. Nicholls and K.A. Dannemann, "Characterization of Confined Intact and Damaged Borosilicate Glass", *J. Amer. Cer. Soc.*, **93**(10): 3390-3398, 2010.
24. P. Patel, M. Motyka, US Army Research Laboratory, Aberdeen, MD, personal communication, Sept. 2005.
25. ASTM E494, "Technique for Measuring Ultrasonic Velocity in Materials", July 2001.
26. Schott Glass, Borofloat 33 Thermal Properties datasheet, <http://www.us.schott.com/borofloat/english/attribute/thermic/index.html>.
27. Starphire Manufacturer Data Sheet – PPG Industries, Inc. <http://www.jnsglass.com/pdf/Starphire.pdf>
28. P. Forquin, A. Arias, and R. Zaera, "An Experimental Method of Measuring the Confined Compression Strength of High-Performance Concretes to Analyse Their Ballistic Behaviour," *J. Phys. IV*, **134**: 629-34, 2006.

UNCLASSIFIED

29. S. Chocron, C.E. Anderson, K.A. Dannemann and A.E. Nicholls, "Characterization of Borosilicate Glass by Confined Compression Testing and Numerical Validation", SwRI Technical Report 18.12544/010, prepared for RDECOM-TARDEC, AMSRD-TAR-R, Warren, MI, November 2009.
30. S. Chocron, C.E. Anderson, K.A. Dannemann and A.E. Nicholls, "Characterization of Soda-Lime Glass by Confined Compression Testing and Numerical Validation", SwRI Technical Report 18.12544/010, prepared for RDECOM-TARDEC, AMSRD-TAR-R, Warren, MI, June 2010.
31. S. Bless, "Using DOP Tests to Evaluate Ballistic Performance of Transparent Material", American Ceramic Society, *35th Int. Conf. on Advanced Ceramics and Composites*, Daytona Beach, FL 2011.
32. S. Chocron, C.E. Anderson, A.E. Nicholls and K.A. Dannemann, "Characterization of Confined Intact and Damaged Soda-Lime Glass", *J. Amer. Cer. Soc.*, submitted, 2011.

UNCLASSIFIED

